Theoretical analysis of the crystal structure, band-gap energy, polarization, and piezoelectric properties of ZnO-BeO solid solutions

L. Dong[1] and S. P. Alpay[1,2,*]

[1] *Department of Physics, University of Connecticut, Storrs, Connecticut 06269, USA*

[2] *Department of Chemical Materials and Biomolecular Engineering and Institute of Materials Science, University of Connecticut, Storrs, Connecticut 06269, USA*

(Received 25 February 2011; revised manuscript received 27 May 2011; published 26 July 2011)

The electrical properties, the spontaneous polarization, and the piezoelectric response of ZnO can be tailored by alloying ZnO with BeO for applications such as electrodes in flat panel displays and solar cells, blue and ultraviolet (UV) light emitting devices, and highly sensitive UV detectors. We present here the results of a study that employs density-functional theory to analyze the crystal structure, the band structure, spontaneous polarization, and piezoelectric properties of $Zn_{1-x}Be_xO$ solid solutions. Our findings indicate that $Zn_{1-x}Be_xO$ alloys may have a different crystal structure than the end components ZnO and BeO that crystallize in the prototypical wurtzite structure ($P6_3mc$). It is shown that orthorhombic lattices with $Pmn2_1$, $Pna2_1$, or $P2_1$ structures may have lower formation energies than the wurtzite lattice at a given Be composition. The band-gap energies of $Zn_{1-x}Be_xO$ in the wurtzite and the orthorhombic structures are nearly identical and the bowing of the band-gap energy increases with increasing Be concentration. The spontaneous polarization of $Zn_{1-x}Be_xO$ in the orthorhombic lattice is markedly larger compared to the wurtzite structure while the piezoelectric polarization in the wurtzite and orthorhombic structures varies linearly with the Be concentration.

DOI: 10.1103/PhysRevB.84.035315 PACS number(s): 77.84.Bw, 71.22.+i, 77.65.−j

I. INTRODUCTION

ZnO thin films and one-dimensional nanostructures have gained significant importance in recent years in electronic, electromechanical, optoelectronic, and magnetic devices.[1–5] This interest stems from the electronic properties including a large direct band gap ($E_g = 3.37$ eV at 300 K), a large exciton binding energy (∼60 meV), strong spontaneous ($P_S = -0.57$ C/m^2) and piezoelectric ($e_{33} = 1.20$ C/m^2, $e_{31} = -0.56$ C/m^2) polarizations, as well as the relative ease of synthesis of ZnO powders, single crystals, thin films, and nanostructures.[1,2,6] Due to these properties, ZnO is a key enabling material in sensors and actuators, transparent thin-film electronics, and optoelectronic and piezoelectric devices.[2,7,8]

Since the electronic properties of ZnO can be readily tuned by doping or alloying, it is possible to expand its applications by designing materials systems for specific conditions and/or restrictions. For example, doping ZnO with Al (1–2%) or Ga (2–7%) results in a solid solution with a high carrier concentration (∼10^{21} cm^{-3}) and a commensurate low electric resistivity (∼10^{-5} Ω cm).[9] Such materials have already been incorporated in flat panel displays and solar cells as transparent electrodes to replace the relatively expensive In-Sn oxide (ITO).[10] ZnO-based multiple quantum well structures such as ultrathin $ZnO/Zn_{1-x}Mg_xO$ multilayers may provide better oscillation strength and enhanced exciton binding energy in blue and ultraviolet (UV) light-emitting devices.[11] As a last example, wider band-gap materials are desired in highly sensitive UV detectors whose cutoff energy falls into a solar-blind energy region from 4.40 to 5.65 eV (220–280 nm), in which the sunlight is absent on earth because of strong atmospheric absorption.[12] There are other materials suitable for this range of wavelength spectrum (e.g., diamond and AlGaN).[13] However, if ZnO-based solid solutions could be developed that would work in this range, this would significantly reduce cost since ZnO is compatible with integrated circuit (IC) and can be synthesized with good stoichiometric control via a number of deposition methods.[14]

Band-gap engineering of ZnO can be achieved by alloying with MgO ($E_g = 7.70$ eV) for UV applications and such alloys can also be used as barrier layers in ZnO/(Zn,Mg)O superlattices for quantum well devices.[15,16] However, phase separation occurs in $Zn_{1-x}Mg_xO$ solid solutions when the Mg composition exceeds 33%.[1,16] This is due to the differences in the crystal structures of ZnO [wurtzite (W), $P6_3mc$] and MgO (rocksalt, $Fm\bar{3}m$). As such, the UV absorption range is limited to 3.37–3.90 eV in the $Zn_{1-x}Mg_xO$ system for $x < 0.33$.[1,12,17] Therefore BeO ($E_g = 10.60$ eV) that also crystallizes in the W structure has been considered as an alloying system for ZnO for UV optoelectronic devices and sensors, despite the high degree of toxicity of elemental Be.[12,17,18] It was shown that $Zn_{1-x}Be_xO$ thin films can be deposited using hybrid beam deposition[19] with no phase separation over the entire composition range.[16] Furthermore, since in $Zn_{1-x}Be_xO$ the band gap can theoretically be tuned from 3.37 to 10.60 eV, this materials system may replace $Zn_{1-x}Mg_xO$ solid solutions that are being considered in applications such as field-effect transistors, polymer-oxide hybrid solar cells, quantum Hall effect devices, high-k films on Si, and acoustic resonators.[20–24]

While there have been some efforts to understand, describe, and measure the lattice parameters, the band gap, and optical properties of $Zn_{1-x}Be_xO$ in thin films,[16,17,25–28] the potential of this materials system for applications described above has not been fully explored. Of particular interest are the following: Would there be any changes in crystal structures of these alloys in one-dimensional nanostructures, where there are only a limited number of anions and cations compared to bulk or thin-film $Zn_{1-x}Be_xO$? Furthermore, considering that these materials are piezoelectric and possess a spontaneous

polarization, how does the polarization change with varying the Be composition in nanostructures where the electrostatics of free surfaces due to termination of atomic bonds play a significant role? To answer these questions and to guide experimental studies, we have carried out first-principles calculations based on the density-functional theory (DFT)[29] with a particular emphasis on the crystal structures, band-gap bowing, spontaneous polarization, and piezoelectric response as a function of the Be composition x. We compare the relative stability and properties of $Zn_{1-x}Be_xO$ solid solutions in the prototypical W structure ($P6_3mc$) and two orthorhombic unit cells with $Pmn2_1/Pna2_1/P2_1$ structures. Our results show that depending on the composition, the alloys may have a different crystal structure than the end components ZnO and BeO. While the electronic structure, the band-gap energy, and the piezoelectric properties are relatively unaffected by the variation in the crystallography of $Zn_{1-x}Be_xO$, the spontaneous polarization shows significant deviations if the crystal structure of the alloy were assumed *a priori* to be the W structure.

II. CRYSTAL STRUCTURES

Both ZnO and BeO have the W structure, which consists of alternating hexagonal closed-packed metal (Zn or Be) and oxygen layers [Fig. 1(a)]. Each metal (oxygen) is nearly equidistant to its four nearest oxygen (metal) atoms which form a tetrahedron. The structure is characterized by an in-plane lattice parameter a_0, an out-of-plane lattice parameter c_0, and an internal lattice parameter u_0 measuring the interatomic distance, i.e., the bond length along the c axis.[30] The atomic size of Zn and the size of the ZnO unit cell are larger than that of Be and BeO (Table I). The W structure and the primitive periodicity of the (0001) layers in the $P6_3mc$ base (hexagonal 1×1 hereafter) are shown in Figs. 1(a) and 1(b), respectively.

Previous DFT simulations assume that $Zn_{1-x}Be_xO$ solid solutions crystallize in the W structure for all x.[17,27] This is based on limited θ-2θ x-ray diffraction (XRD) experiments on epitaxial or highly oriented $Zn_{1-x}Be_xO$ films grown on the (0001) α-Al_2O_3 substrates.[16,25,31] XRD results show that the out-of-plane lattice parameter of $Zn_{1-x}Be_xO$ films varies linearly with increasing x.[16] However, information regarding other structural or crystallographic properties, such as the relative atomic positions and symmetry in the basal plane, that are needed to completely characterize the crystal structure of these alloys is lacking. Such factors play a significant role on the growth morphology, band structure, spontaneous polarization, and piezoelectric properties of a material. Provided that the same interlayer distance along the c axis is maintained, crystal structures other than the W lattice may indeed become possible, especially in one-dimensional nanostructures. As an example, we point to recent calculations in the (In,Ga)N system showing that certain orthorhombic lattices that are obtained by breaking the in-plane hexagonal symmetry of the (0001) layers of the W unit cell may become energetically favorable.[32,33] We present in Figs. 1(c) and 1(d) the basal planes of two different unit cells for the $Zn_{0.5}Be_{0.5}O$ composition, both of which can be constructed from Fig. 1(b). Figure 1(c) corresponds to a hexagonal 2×2 or a rectangular $1\times\sqrt{3}$ base that generates a W lattice

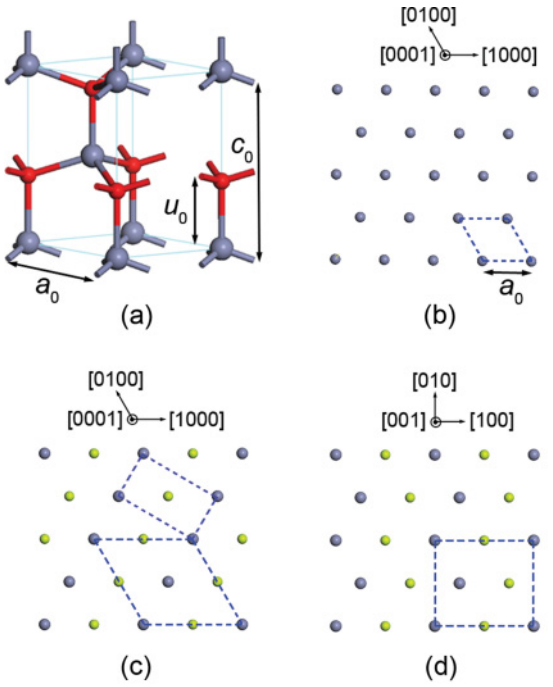

FIG. 1. (Color online) (a) Wurtzite (W) unit cell of ZnO; the planar view along the c axis of (b) W ZnO, (c) W $Zn_{0.5}Be_{0.5}O$, and (d) O-16 $Zn_{0.5}Be_{0.5}O$. The base of each structure in (b), (c), and (d) is shown by dashed lines.

TABLE I. Calculated and experimental values of the structural parameters a_0, c_0/a_0, and u_0, the band-gap energy E_g, and the spontaneous polarization P_S of ZnO and BeO in the W structure.

		a_0 (Å)	c_0/a_0	u_0	E_g (eV)	P_S (C/m^2)
ZnO	this work	3.277	1.616	0.3787	0.758	−0.031
	other DFT	3.183[a]	1.620[a]	0.379,[a]0.383[b]	0.804[c]	−0.029,[a] − 0.057[b]
	experimental	3.250	1.603	0.382	3.37	
BeO	this work	2.710	1.626	0.3773	7.509	−0.035
	other DFT	2.688[b]	1.619[b]	0.379[b]	7.36[d]	−0.036[b]
	experimental	2.698	1.622	0.378	10.6	

[a]Reference 41.
[b]Reference 42.
[c]Reference 43.
[d]Reference 44.

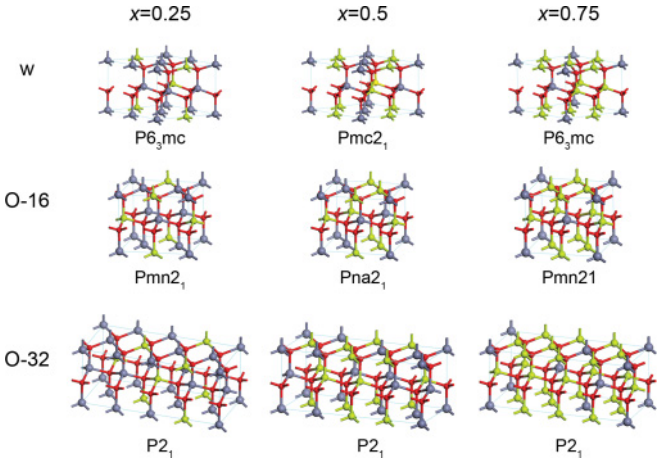

FIG. 2. (Color online) Supercells of $Zn_{1-x}Be_xO$ solid solutions in the W, O-16, and O-32 structures for Be compositions $x = 0.25$, 0.50, and 0.75. Also shown are the space groups of each structure.

but with $Pmc2_1$ symmetry, where as Fig. 1(d) is a rectangular $2 \times \sqrt{3}$ base that may produce a $Pna2_1$ unit cell. This way one can envision composition-dependent supercells that have orthorhombic symmetry, in addition to the prototypical W structure.

In Fig. 2 we provide the possible crystal structures and space groups of the compositions that were considered in this study. These are (i) the W structure ($P6_3mc$ or $Pmc2_1$), (ii) orthorhombic O-16 structures ($Pmn2_1$ or $Pna2_1$), and (iii) orthorhombic O-32 structures ($P2_1$). The basal plane of the W, O-16, and O-32 are hexagonal 2×2, rectangular $2 \times \sqrt{3}$, rectangular $4 \times \sqrt{3}$, respectively. All unit cells retain the same periodicity as ZnO or BeO along the c axis. Since there are eight atoms in the basal plane in O-32, this allows us to model several other compositions with $x = 0.125$, 0.375, 0.625, and 0.875 (Fig. 3).

III. COMPUTATIONAL METHODS

Calculations were carried out at 0 K using the PW91 generalized gradient approximation (GGA)[34] of DFT as implemented in Vienna *ab initio* Simulation Package (VASP).[35] The plane-wave pseudopotentials based on the projector-augmented wave method were used[36] and the wave functions were expanded with an energy cutoff of 500 eV. We note that the Zn $3d$ electrons are explicitly included in the valence states. Previous DFT calculations on ZnXO (X = Cd, Mg, or Be) and GaZN (Z = Al or In) alloys[17,27,32,33,37,38] show that each supercell of the alloy structure containing 16 (W and O-16) or 32 (O-32) atoms is sufficiently large to give the ground-state configurations. For pure ZnO and BeO, a $9 \times 9 \times 6$ Γ-centered k-point mesh in the first Brillouin zone was found to yield well converged results. For the alloy supercells, $5 \times 5 \times 6$, $5 \times 6 \times 6$, $3 \times 6 \times 6$ Γ-centered k-point meshes were employed for the W, O-16, and O-32 lattices, respectively. The atomic positions in the supercells were optimized until all components of the force on each atom were reduced to values below 0.02 eV/Å. The polarizations were calculated using the Berry-phase approach[39] where a reference phase with zero net polarization is needed. This reference phase was taken to be the zinc-blende structure ($F\bar{4}\,3m$) because it is centrosymmetric and has thus no net polarization. The polarization of the W, O-16, and O-32 phases were obtained by comparing these to the reference by employing the methodology described by Bernardini, Fiorentini, and Vanderbilt.[40]

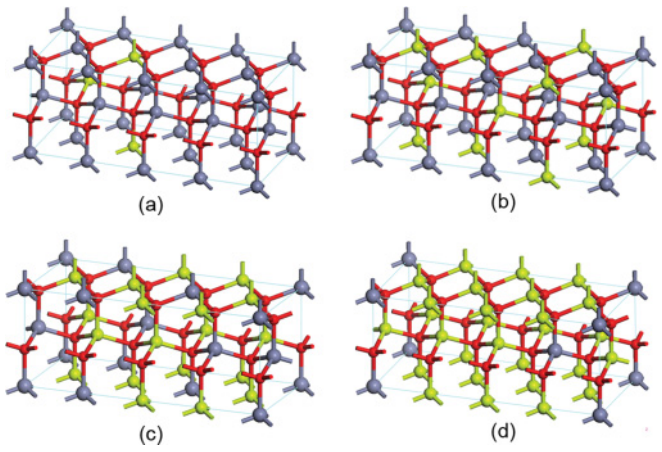

FIG. 3. (Color online) $P2_1$ crystal structures of O-32 $Zn_{1-x}Be_xO$ alloys for (a) $x = 0.125$, (b) $x = 0.375$, (c) $x = 0.625$, and (d) $x = 0.875$.

IV. RESULTS AND DISCUSSION

A. End components ZnO and BeO

The fundamental properties of ZnO and BeO in the W phase have been studied extensively via DFT.[41–44] We provide in Table I previously obtained experimental and theoretical values for the lattice parameters, band-gap energy, and spontaneous polarization of ZnO and BeO. Table I shows that our calculated lattice parameters a_0 and c_0 for both ZnO and BeO are in good agreement with the data in the literature. The electronic structures of ZnO and BeO display a direct bang gap in the Γ point of the first Brillouin zone. Similar to other DFT results, theoretical band-gap energies are lower than the experimental values (0.758 eV, cf. 3.37 eV for ZnO and 7.509 eV, cf. 10.6 eV for BeO). Although experimental E_g can be reproduced by more recent time-intensive beyond DFT calculations,[43,45] the relatively simpler GGA is employed in our analysis. This is primarily done to focus on the *relative variations* in E_g of the alloys with respect to pure ZnO and BeO, noting that such changes in E_g can be predicted accurately via DFT.

The positive direction of the spontaneous polarization P_S is conventionally defined as pointing from the O atom to its nearest-neighboring Zn or Be atom along the [0001] direction. There are two distinct contributions from the W unit cells of ZnO and BeO to P_S: the lack of centrosymmetry, and the deviation from the ideal W unit cell for which $c/a \cong 1.633$ and $u = 0.375$. Obviously, there is a strong correlation between u, which is the bonding length between the Zn (Be) and O atoms along [0001] and P_S (Table I). For ZnO our calculations yield $u_0 = 0.379$, which is closer to the ideal value of u (for which $P_S = 0$), resulting in $P_S = -0.031$ C/m^2. This is in agreement with one theoretical finding (-0.029 C/m^2)[41] and significantly smaller than another calculation (-0.057 C/m^2).[42]

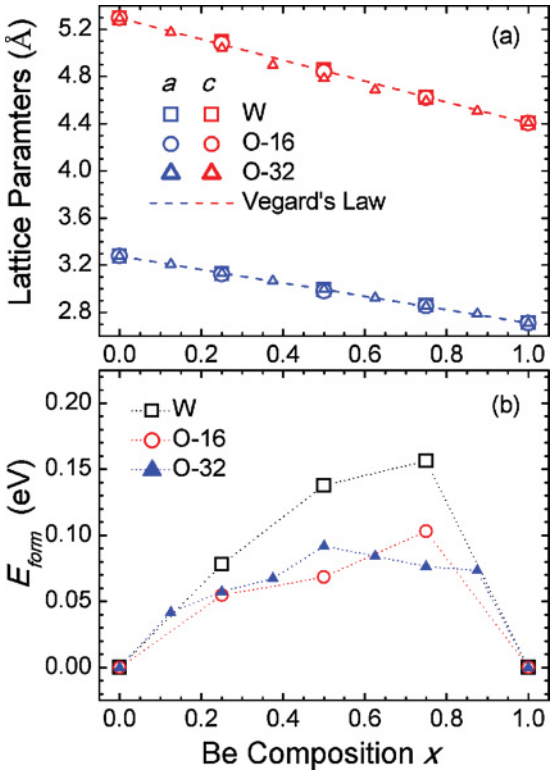

FIG. 4. (Color online) (a) Equilibrium lattice parameters a_0 and c of $Zn_{1-x}Be_xO$ solid solutions in the W 1 × 1 base and (b) formation energy of the W, O-16, and O-32 structures as a function of Be concentration.

B. Lattice parameters and formation energies

The lattice parameters of $Zn_{1-x}Be_xO$ as a function of x in the W, O-16, and O-32 structures are plotted in Fig. 4(a). For a more meaningful comparison of these crystal structures, we use the equivalent in-plane lattice parameter a_0 in the hexagonal 1 × 1 format [(Fig. 1(b)]. Despite different in-plane symmetries and atomic arrangements, the lattice parameters a_0 and c of the three structures have nearly identical values at a given Be composition x and obey Vegard's law,

$$a_0(Zn_{1-x}Be_xO) = xa_0(BeO) + (1-x)a_0(ZnO), \quad (1)$$

$$c(Zn_{1-x}Be_xO) = xc(BeO) + (1-x)c(ZnO), \quad (2)$$

where Eq. (2) is in agreement with the experimental measurements of Ryu *et al.*[16]

The relative stability of the structure of a particular $Zn_{1-x}Be_xO$ composition is determined by its formation energy per cation-anion pair at 0 K given by[17]

$$E_{form}(Zn_{1-x}Be_xO) = E(Zn_{1-x}Be_xO) - xE(BeO) - (1-x)E(ZnO), \quad (3)$$

which is essentially the difference between the total internal energies of formation of $Zn_{1-x}Be_xO$ and the weighed internal energies of formations of ZnO and BeO. E_{form} can be related to the lattice distortions arising from interatomic interactions in the W, O-16, and O-32 structures. Due to the different atomic sizes of Zn and Be, the position of each atom deviates slightly from that of a pure ZnO or BeO in the W, O-16, or O-32 lattice. As a consequence, the O tetrahedron surrounding each Zn (Be) atom is deformed, so that the four Zn-O (Be-O) bonding lengths within the tetrahedron are no longer equidistant and their average value changes from that of pure ZnO (BeO). As such, $Zn_{1-x}Be_xO$ alloy requires additional bonding energy, which is qualitatively proportional to the square of the percent variation in the average Zn-O and Be-O bonding lengths compared to bulk ZnO and BeO (Table II).

TABLE II. Percent variation in the average Zn-O and Be-O bonding lengths in the W, O-16, and O-32 alloys compared to bulk ZnO and BeO.

	W		O−16		O−32	
	Zn-O	Be-O	Zn-O	Be-O	Zn-O	Be-O
$Zn_{0.875}Be_{0.125}O$					0.07	1.89
$Zn_{0.75}Be_{0.25}O$	0.19	1.86	0.11	1.06	0.09	1.33
$Zn_{0.625}Be_{0.375}O$					0.1	1.13
$Zn_{0.5}Be_{0.5}O$	−0.71	2.08	0.00	1.00	−0.13	1.38
$Zn_{0.375}Be_{0.625}O$					−0.28	1.13
$Zn_{0.25}Be_{0.75}O$	−2.73	1.86	−1.55	1.33	−0.65	0.95
$Zn_{0.125}Be_{0.875}O$					−2.16	0.79

Furthermore, Be-O bonds are stronger than the Zn-O bonds, simply considering the fact that the bulk modulus of BeO is almost double that of ZnO.[1,46] The reason for this is the larger number of electrons in Zn^{2+}. For a given percent variation, the formation of Be-O bonds would require higher energy than the formation of Zn-O bonds. Thus E_{form} in the alloys is mainly determined by the length variation of the Be-O bonds. The magnitude of percent variation of average Be-O bonding length in the W structure is almost twice as large as that in the O-16 and O-32 structures for $x = 0.25$, 0.5, and 0.75 (Table II). As seen in Fig. 4(b), this agrees well with the much larger E_{form} in W structures.

As x varies from 0 to 1, Zn-O bonds are gradually replaced by Be-O bonds in $Zn_{1-x}Be_xO$. Hence for a given alloy structure, if the length variation in Be-O and Zn-O bonds remains constant as a function of x, E_{form} would still increase

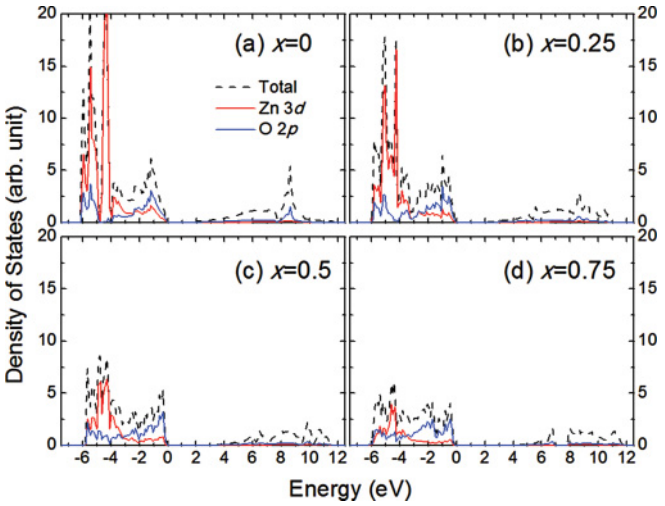

FIG. 5. (Color online) Electronic density of states of $Zn_{1-x}Be_xO$ at (a) $x = 0$, (b) $x = 0.25$, (c) $x = 0.5$, and (d) $x = 0.75$. Maximum of the valence bands is set to be 0 eV for each concentration.

from $x = 0.25$ to $x = 0.75$. This is the case in the W and O-16 structures. The slope of the increase in E_{form} in the O-16 structure is smaller compared to that in the W structure, due to a smaller value of bond length variation. However, E_{form} in the O-32 structure shows a slight decrease in the range $0.5 < x < 0.875$, because the increase in the number of Be-O bonds is partially compensated by the reduction in the magnitude of variation in Be-O bonding lengths in this composition range.

C. Electronic structure

The electronic band structures (not shown) and density of states of ZnO and BeO in our study agree well with previous experimental and theoretical studies (taking into account the underestimation in DFT).[43,47] The band gap originates from the bonding-antibonding interaction between Zn 3*s* (Be 2*s*) electrons, which dominate the bottom of the conduction bands (CBs), and O 2*p* electrons, which dominate the top of the valence bands (VBs). Compared to that of BeO, VBs of ZnO have an additional (and relatively large) contribution from the Zn 3*d* electrons [Fig. 5(a)]. The strong O 2*p* and Zn 3*d* hybridization in ZnO results in two major effects: (i) the top of VBs are shifted closer to the Zn 4*s* states, reducing the band-gap energy; (ii) the original narrow Zn 3*d* bands are significantly dispersed (−3.9 to −6.2 eV) and separated into two groups of peaks around −4.3 and −5.4 eV. For the solid solutions, as x increases from 0 to 1, the Zn 3*d* contribution and hence the *p*-*d* repulsion is continuously weakened [Figs. 5(b)–5(d)]. The lower Zn 3*d* peak (−5.4 eV) gradually decreases and disappears completely for BeO. The density of states for the compositions analyzed in this study does not display a discernible change for the three different crystal structures considered here.

The band-gap energies of the alloys for the three structures as a function of x are plotted in Fig. 6(a). Similar to the lattice parameters, E_g is nearly the same for the W, O-16, and O-32 configurations at a given x. Over the entire composition range, E_g displays a nonlinear dependence on x, which can be described using a parabolic approximation:

$$E_g(\text{Zn}_{1-x}\text{Be}_x\text{O}) = xE_g(\text{BeO}) + (1-x)E_g(\text{ZnO}) - bx(1-x), \quad (4)$$

where b is the bowing parameter. Average values of b ($\langle b \rangle$) for the W, O-16, and O-32 structures are 6.17, 5.54, and 5.33 eV, respectively, which are consistent with the result in Ref. 27. Compared to the linear interpolation of E_g in $\text{Zn}_{1-x}\text{Mg}_x\text{O}$ alloys with $0 < x < 0.33$,[48] $\langle b \rangle$ of $\text{Zn}_{1-x}\text{Be}_x\text{O}$ is significantly larger due to the large size difference between Zn^{2+} (0.74 Å) and Be^{2+} (0.45 Å).[49] However, further analysis of the data shown in Fig. 6(a) indicates that a single average bowing parameter over the whole composition range is not sufficient to describe the dependence of E_g as a function of x. In Fig. 6(b), we plot $b(x)$ in the O-32 structure as a function of the Be concentration. $b(x)$ is smaller than $\langle b \rangle$ and is relatively composition independent until $x = 0.5$ [$b(x) \sim 4.5$ eV]. It increases sharply with x from ~5.0 eV at $x = 0.5$ to ~13.0 eV for $x = 0.875$. The larger value of $b(x)$ in Be-rich alloys is due to the additional interaction resulting from the 3*d* Zn^{2+} and 2*p* O^{2-} repulsions that shift the valence band up.[28] Although E_g is typically underestimated in DFT calculations, the trend in the variation in $b(x)$ is in good agreement with experimental results [Fig. 6(b)] derived from the measured E_g of alloys in Ref. 16.

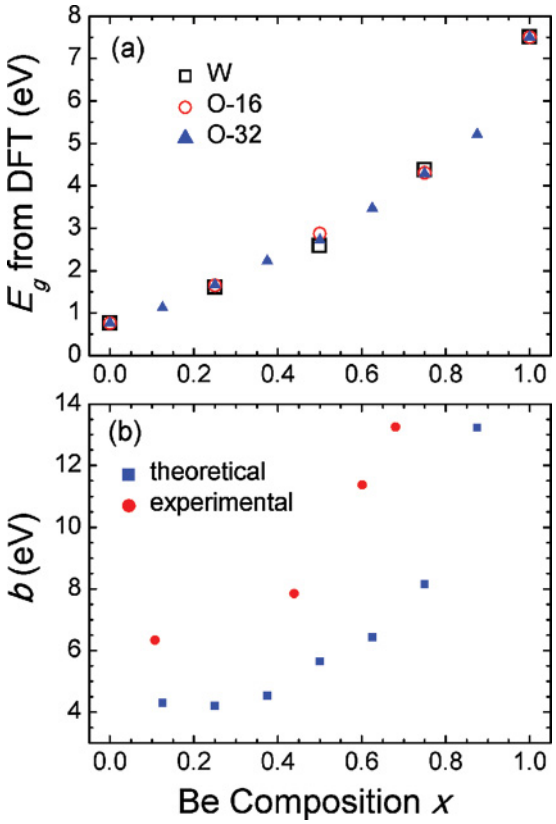

FIG. 6. (Color online) (a) Band-gap energy (E_g) of $\text{Zn}_{1-x}\text{Be}_x\text{O}$ solutions from DFT calculations and (b) theoretical band-gap bowing parameter $b(x)$ of the O-32 structure as a function of the Be concentration derived from the theoretical E_g together with the experimental bowing parameter obtained from the measured E_g in Ref. 16.

D. Spontaneous polarization and piezoelectric properties

The particular shape of nanostructures of polarizable piezoelectric materials depends closely on the crystal structure and the magnitude and orientation of the spontaneous polarization. Several different nanostructures of ZnO (such as nanohelixes, nanospirals, and nanorings)[2,50] have been synthesized using these principles. In this section, we calculate the spontaneous polarization of $\text{Zn}_{1-x}\text{Be}_x\text{O}$ alloys in the W, O-16, and O-32 lattices by comparing these with the reference zinc-blende structure [Fig. 7(a)]. Our results show that for all three structures, P_S deviates from the Vegard's linear approximation.

P_S of $\text{Zn}_{1-x}\text{Be}_x\text{O}$ in the W structure as a function of Be composition x can be described via a parabolic function given by

$$P_S(\text{Zn}_{1-x}\text{Be}_x\text{O}) = xP_S(\text{BeO}) + (1-x)P_S(\text{ZnO}) - b_S x(1-x), \quad (5)$$

where the polarization bowing parameter b_S is $-0.0916\ \text{C/m}^2$. Figure 7(a) shows that $P_S(x)$ in the W structure is significantly less in magnitude than the weighted averages of P_S of ZnO

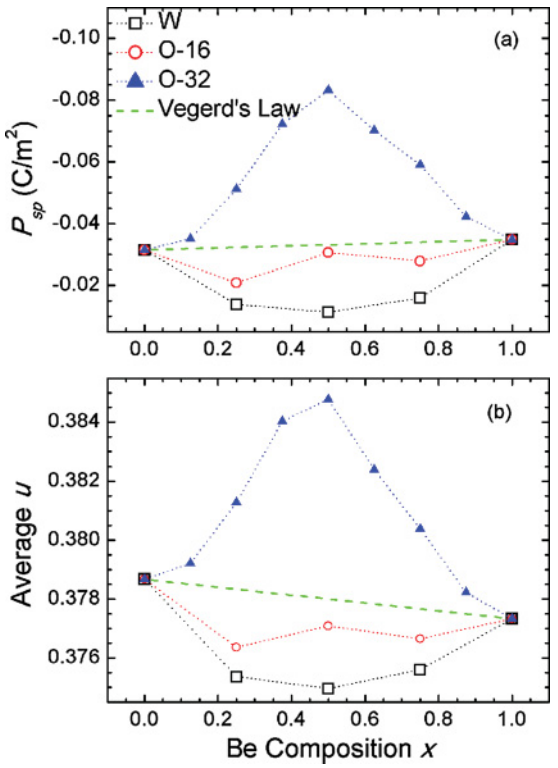

FIG. 7. (Color online) (a) Spontaneous polarization and (b) the average internal lattice parameter of the W, O-16, and O-32 structures as a function of the Be concentration.

and BeO; for $x = 0.5$, $P_S = -0.011$ C/m^2 compared to the Vegard's law approximation of -0.033 C/m^2. On the other hand, O-32 structures have higher polarization throughout the composition range that was investigated in this study. The largest difference occurs at $x = 0.5$ for which P_S are -0.011 C/m^2 and -0.083 C/m^2 in the W and O-32 structures, respectively.

Since P_S (along the c axis) arises from relative displacements of the anions and cations, it is closely related to the bonding length along this direction. In Fig. 7(b), we plot the average value of bonding lengths along the c axis ($\bar{u}$) in the W, O-16, and O-32 structures as a function of x. The correlation between $\bar{u}$ and P_S is obvious and can be attributed to an internal strain effect resulting from the variation of Zn-O and Be-O bond lengths in the alloys.[37] The fluctuation of P_S agrees with that of $\bar{u}$ in the O-16 structure. In W and O-16 structures, this internal strain is compressive so that the average bonds are shortened along the c axis. As a comparison, the internal tensile strain in the O-32 structure results in a relatively large elongation of bonds in the same direction. The strength of this internal strain is proportional to the deviation of $\bar{u}(x)$from the Vegard's law prediction: it is strongest in the O-32 structure and weakest in O-16.

Besides internal strains, there might be two other distinct effects resulting in nonlinear interpolation of P_S in the alloys: the volume deformation of the parent binaries, which are compressed or stretched from their individual equilibrium lattices to the alloy values; and the chemical disorder effects due to the random distribution of metal on the cation sites.[37] The relative contribution of these can be estimated in O-16 $Zn_{0.5}Be_{0.5}O$ for which the internal strain effect is negligible since $\bar{u}$ is close to the linear approximation. Since the bowing of P_S of it is small, one can conclude that in the $Zn_{1-x}Be_xO$ alloy system, the contributions of the volume deformation and chemical disorder on P_S are not as significant as the internal stain effect. Furthermore, these two effects would not result in any discrepancy in P_S of the W, O-16, or O-32 alloys at a given Be concentration. This is a straightforward conclusion considering (i) these structures have almost identical lattice parameters [Fig. 4(a)]; (ii) they have the same periodicity along the polarization direction (c axis) despite different in-plane symmetries; and (iii) each O atom in the W and O-16 structures has to be surrounded by Zn *and* Be atoms commensurate with its stoichiometry (Fig. 2).

Piezoelectric polarization (P_{PZ}) results from external strain ε_j, which can be expressed as

$$P_{PZ} = \sum_j e_{ij}\varepsilon_j, \tag{6}$$

where e_{ij} are the components of the piezoelectric tensor in Voigt notation.[40] In the W structure, P_{PZ} along the c axis is reduced to[40]

$$P_{PZ}^{W} = e_{31}^{W}(\varepsilon_1 + \varepsilon_2) + e_{33}^{W}\varepsilon_3 = 2e_{//}^{W}\varepsilon_{//} + e_{33}^{W}\varepsilon_3, \tag{7}$$

where $\varepsilon_{//} = \varepsilon_1 = \varepsilon_2$ is the equibiaxial in-plane strain, ε_3 is the strain along the c axis, and $e_{//}^{W} = e_{31}^{W}$. The calculated piezoelectric coefficients of ZnO ($e_{31} = -0.58$ C/m^2, $e_{33} = 1.20$ C/m^2) and BeO ($e_{31} = -0.14$ C/m^2, $e_{33} = 0.22$ C/m^2) agree well with experimental and other DFT results.[1,41,42,51]

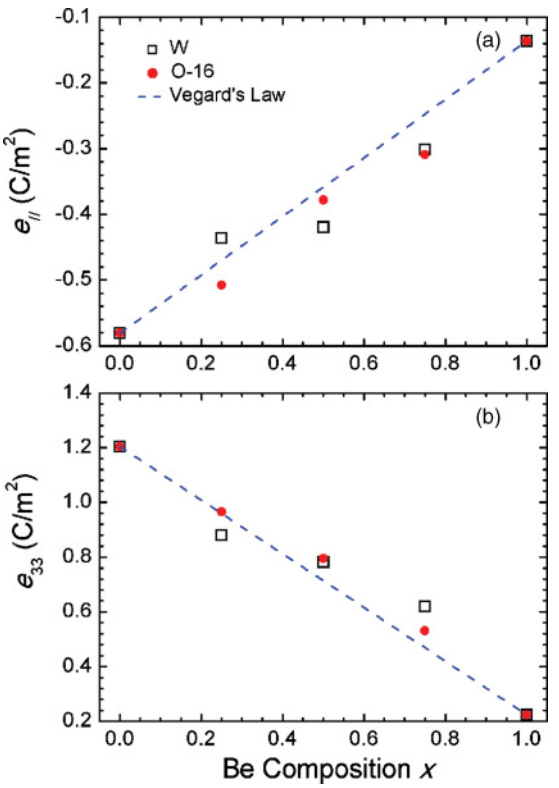

FIG. 8. (Color online) Piezoelectric polarization (a) $e_{//}$ and (b) e_{33} of the W and O-16 structures as a function of the Be concentration.

On the other hand, in the O-16 structures[52]

$$P_{PZ}^{O-16} = e_{31}^{O-16}\varepsilon_1 + e_{32}^{O-16}\varepsilon_2 + e_{33}^{O-16}\varepsilon_3 = \left(e_{31}^{O-16} + e_{32}^{O-16}\right)\varepsilon_{//} + e_{33}^{O-16}\varepsilon_3. \quad (8)$$

To compare the piezoelectric response of the W and O-16 structures, we use an effective coefficient $e_{//}^{O-16} = (e_{31}^{O-16} + e_{32}^{O-16})/2$ in the O-16 structure such that

$$P_{PZ}^{O-16} = 2e_{//}^{O-16}\varepsilon_{//} + e_{33}^{O-16}\varepsilon_3. \quad (9)$$

The calculated piezoelectric coefficients $e_{//}$ and e_{33} for both the W and O-16 structures show a roughly linear interpolation with the Be concentration x (Fig. 8).

V. CONCLUSIONS

We have used DFT to study the crystal structure, band-gap bowing, spontaneous polarization, and piezoelectric response of $Zn_{1-x}Be_xO$ solid solutions. Our results show $Zn_{1-x}Be_xO$ alloys have different crystal structures than the end components ZnO and BeO, which have a W unit cell with a 2×2 in-plane hexagonal symmetry. The calculations demonstrate that orthorhombic O-16 and O-32 structures with rectangular $2 \times \sqrt{3}$ or $4 \times \sqrt{3}$ in-plane symmetry, respectively, are energetically more favorable over the W structure at given Be composition. The band-gap energies of $Zn_{1-x}Be_xO$ in the W, O-16, and O-32 structures are nearly identical and display strong bowing; the bowing parameter varies from 4.5 to 13.0 eV as x varies from 0.125 to 0.875. The spontaneous polarization of $Zn_{1-x}Be_xO$ for all three structures deviates significantly from the Vegard's law. This is related to the lengths of Zn-O and Be-O bonds along the (0001)/(001) direction. The piezoelectric polarization coefficients e_{31} and e_{33} in both the W and the O-16 structures follow Vegard's law.

ACKNOWLEDGMENTS

This work was partially supported by the US Department of Energy under Grant No. DE-EE0000210. The authors also thank P.-X. Gao and R. Ramprasad at the University of Connecticut for many illuminating discussions.

*p.alpay@ims.uconn.edu

[1] U. Ozgur, Y. I. Alivov, C. Liu, A. Teke, M. A. Reshchikov, S. Dogan, V. Avrutin, S. J. Cho, and H. Morkoc, J. Appl. Phys. **98**, 041301 (2005).
[2] Z. L. Wang, X. Y. Kong, Y. Ding, P. Gao, W. L. Hughes, R. Yang, and Y. Zhang, Adv. Funct. Mater. **14**, 943 (2004).
[3] M. H. Huang, S. Mao, H. Feick, H. Yan, Y. Wu, H. Kind, E. Weber, R. Russo, and P. Yang, Science **292**, 1897 (2001).
[4] S. J. Pearton, C. R. Abernathy, M. E. Overberg, G. T. Thaler, D. P. Norton, N. Theodoropoulou, A. F. Hebard, Y. D. Park, F. Ren, J. Kim, and L. A. Boatner, J. Appl. Phys. **93**, 1 (2003).
[5] C. R. Gorla and N. W. Emanetoglu, J. Appl. Phys. **85**, 2595 (1999).
[6] D. Karanth and H. Fu, Phys. Rev. B **72**, 064116 (2005).
[7] E. M. C. Fortunato, P. M. C. Barquinha, A. C. M. B. G. Pimentel, A. M. F. Goncalves, A. J. S. Marques, L. M. N. Pereira, and R. F. P. Martins, Adv. Mater. **17**, 590 (2005).
[8] J.-H. Lim, C.-K. Kang, K.-K. Kim, I.-K. Park, D.-K. Hwang, and S.-J. Park, Adv. Mater. **18**, 2720 (2006).
[9] T. Minami, Semicond. Sci. Technol. **20**, S35 (2005).
[10] C. Klingshirn, Phys. Status Solidi **244**, 3027 (2007).
[11] H. D. Sun, T. Makino, Y. Segawa, M. Kawasaki, A. Ohtomo, K. Tamura, and H. Koinuma, J. Appl. Phys. **91**, 1993 (2002).
[12] C. Yang, X. M. Li, Y. F. Gu, W. D. Yu, X. D. Gao, and Y. W. Zhang, Appl. Phys. Lett. **93**, 112114 (2008).
[13] K. Liu, M. Sakurai, and M. Aono, Sensors **10**, 8604 (2010).
[14] M. J. Vellekoop, C. C. O. Visser, P. M. Sarro, and A. Venema, Sensors and Actuators A: Physical **23**, 1027 (1990).
[15] T. Makino, Y. Segawa, M. Kawasaki, A. Ohtomo, R. Shiroki, K. Tamura, T. Yasuda, and H. Koinuma, Appl. Phys. Lett. **78**, 1237 (2001).
[16] Y. R. Ryu, T. S. Lee, J. A. Lubguban, A. B. Corman, H. W. White, J. H. Leem, M. S. Han, Y. S. Park, C. J. Youn, and W. J. Kim, Appl. Phys. Lett. **88**, 052103 (2006).
[17] X. F. Fan, Z. Zhu, Y. S. Ong, Y. M. Lu, Z. X. Shen, and J. L. Kuo, Appl. Phys. Lett. **91**, 121121 (2007).
[18] Y. R. Ryu, J. A. Lubguban, T. S. Lee, H. W. White, T. S. Jeong, C. J. Youn, and B. J. Kim, Appl. Phys. Lett. **90**, 131115 (2007).
[19] Y. R. Ryu, T. S. Lee, and H. W. White, J. Cryst. Growth **261**, 502 (2004).
[20] M. Nakano, A. Tsukazaki, A. Ohtomo, K. Ueno, S. Akasaka, H. Yuji, K. Nakahara, T. Fukumura, and M. Kawasaki, Adv. Mater. **22**, 876 (2010).
[21] D. C. Olson, S. E. Shaheen, M. S. White, W. J. Mitchell, M. F. A. M. van Hest, R. T. Collins, and D. S. Ginley, Adv. Funct. Mater. **17**, 264 (2007).
[22] A. Tsukazaki, S. Akasaka, K. Nakahara, Y. Ohno, H. Ohno, D. Maryenko, A. Ohtomo, and M. Kawasaki, Nat. Mater. **9**, 889 (2010).
[23] J. Liang, H. Wu, N. Chen, and T. Xu, Semicond. Sci. Tech. **20**, L15 (2005).
[24] Y. Chen, P. Reyes, Z. Duan, G. Saraf, R. Wittstruck, Y. Lu, O. Taratula, and E. Galoppini, J. Electron. Mater. **38**, 1605 (2009).
[25] T. S. Jeong, M. S. Han, J. H. Kim, S. J. Bae, and C. J. Youn, J. Phys. D **40**, 370 (2007).
[26] J. M. Khoshman, D. C. Ingram, and M. E. Kordesch, Appl. Phys. Lett. **92**, 091902 (2008).
[27] S. F. Ding, G. H. Fan, S. T. Li, K. Chen, and B. Xiao, Physica B **394**, 127 (2007).
[28] H. L. Shi and Y. Duan, Eur. Phys. J. B **66**, 439 (2008).
[29] W. Kohn, A. D. Becke, and R. G. Parr, J. Phys. Chem. **100**, 12974 (1996).
[30] L. Dong, S. K. Yadav, R. Ramprasad, and S. P. Alpay, Appl. Phys. Lett. **96**, 202106 (2010).
[31] W. J. Kim, J. H. Leem, M. S. Han, I.-W. Park, Y. R. Ryu, and T. S. Lee, J. Appl. Phys. **99**, 096104 (2006).
[32] H. J. Xiang, S. H. Wei, J. L. F. Da Silva, and J. Li, Phys. Rev. B **78**, 193301 (2008).
[33] H. J. Xiang, S. H. Wei, S. Y. Chen, and X. G. Gong, Phys. Rev. B **80**, 113201 (2009).

[34]J. P. Perdew, J. A. Chevary, S. H. Vosko, K. A. Jackson, M. R. Pederson, D. J. Singh, and C. Fiolhais, Phys. Rev. B **46**, 6671 (1992).
[35]G. Kresse and J. Furthmuller, Phys. Rev. B **54**, 11169 (1996).
[36]P. E. Blochl, Phys. Rev. B **50**, 17953 (1994).
[37]F. Bernardini and V. Fiorentini, Phys. Rev. B **64**, 085207 (2001).
[38]Y. Z. Zhu, G. D. Chen, H. Ye, A. Walsh, C. Y. Moon, and S.-H. Wei, Phys. Rev. B **77**, 245209 (2008).
[39]R. D. King-Smith and D. Vanderbilt, Phys. Rev. B **47**, 1651 (1993).
[40]F. Bernardini, V. Fiorentini, and D. Vanderbilt, Phys. Rev. B **56**, R10024 (1997).
[41]Y. Noel, M. Llunell, R. Orlando, P. D'Arco, and R. Dovesi, Phys. Rev. B **66**, 214107 (2002).
[42]Y. Noel, C. M. Zicovich-Wilson, B. Civalleri, P. D'Arco, and R. Dovesi, Phys. Rev. B **65**, 014111 (2001).
[43]B. Baumeier, P. Kruger, and J. Pollmann, Phys. Rev. B **75**, 045323 (2007).
[44]S. Z. Karazhanov, P. Ravindran, A. Kjekhus, H. Fjellvag, U. Grossner, and B. G. Svensson, J. Cryst. Growth **287**, 162 (2006).
[45]S. Lany and A. Zunger, Phys. Rev. B **81**, 113201 (2010).
[46]V. Milman and M. C. Warren, J. Phys.: Condens. Matter **13**, 241 (2001).
[47]P. Schroer, P. Kruger, and J. Pollmann, Phys. Rev. B **47**, 6971 (1993).
[48]N. B. Chen and C. H. Sui, Mater. Sci. Eng. B **126**, 16 (2006).
[49]R. Shannon, Acta Crystallogr., Sect. A **32**, 751 (1976).
[50]X. Y. Kong and Z. L. Wang, Nano Lett. **3**, 1625 (2003).
[51]S. B. Austerman, D. A. Berlincourt, and H. H. A. Krueger, J. Appl. Phys. **34**, 339 (1963).
[52]J. F. Nye, *Physical Properties of Crystals: Their Representation by Tensors and Matrices* (Oxford University Press, London, 1957).